



**HAL**  
open science

## A Discrete Element Method based-approach for arched masonry structures under blast loads

Filippo Masi, Ioannis Stefanou, Victor Maffi-Berthier, Paolo Vannucci

### ► To cite this version:

Filippo Masi, Ioannis Stefanou, Victor Maffi-Berthier, Paolo Vannucci. A Discrete Element Method based-approach for arched masonry structures under blast loads. *Engineering Structures*, 2020, 216, 10.1016/j.engstruct.2020.110721 . hal-02320696v1

**HAL Id: hal-02320696**

**<https://hal.science/hal-02320696v1>**

Submitted on 19 Oct 2019 (v1), last revised 25 May 2020 (v2)

**HAL** is a multi-disciplinary open access archive for the deposit and dissemination of scientific research documents, whether they are published or not. The documents may come from teaching and research institutions in France or abroad, or from public or private research centers.

L'archive ouverte pluridisciplinaire **HAL**, est destinée au dépôt et à la diffusion de documents scientifiques de niveau recherche, publiés ou non, émanant des établissements d'enseignement et de recherche français ou étrangers, des laboratoires publics ou privés.

# Micro-modelling of non-standard masonry structures under blast loads

Filippo Masi<sup>a,b</sup>, Ioannis Stefanou<sup>a</sup>, Victor Maffi-Berthier<sup>b</sup>, Paolo Vannucci<sup>c</sup>

<sup>a</sup>*Laboratoire Navier, UMR 8205, École des Ponts, IFSTTAR, CNRS, UPE,  
6-8 avenue Blaise Pascal, F-77455, Champs-sur-Marne, France.*

<sup>b</sup>*Ingérop Conseil et Ingénierie,  
18 rue des Deux Gares, F-92500, Rueil-Malmaison, France.*

<sup>c</sup>*LMV, UMR 8100, Université de Versailles et Saint-Quentin,  
55 avenue de Paris, F-78035, Versailles, France.*

Masonry structures are often characterized by complex, non-planar geometries. This is also the case for historical and monumental structures. Here we investigate the dynamic behaviour of non-standard, curvilinear masonry geometries, such as vaults, subjected to blast loading.

We use the Discrete Element Method (DEM) for modelling the dynamic structural response to explosions. The approach allows considering the detailed mechanical and geometrical characteristics of masonry, as well as the inherent coupling between the in- and out-of-plane motion.

The proposed modelling approach is validated with existing experimental tests in the case of planar masonry geometries, i.e., walls, subjected to far-field explosions. The DEM model predicts very well the dynamic response of the system and the failure mode.

Then the response of a typical curved masonry structure subjected to blast loading is investigated. The influence of various micro-mechanical parameters, such as the dilatancy angle, the tensile strength and the cohesion of the masonry joints on the overall dynamic structural response of the system is explored. The effect of the size of the building blocks is also studied.

Masonry joints with zero dilatancy lead to increased out-of-plane deformations with respect to the associative case. Cohesion and tensile strength are found to have negligible influence on the structural response for this type of loading, while the larger the building blocks are the greater the strength of the system is.

Finally, the pertinence of assuming infinitely rigid blocks in the DEM simulations is explored and evaluated through detailed comparisons of the parametric numerical tests using deformable blocks. The predictions of a rigid blocks model are inexact due to rotational locking.

*Keywords:* Masonry; Discrete Element Method (DEM); Blast load; Dilatancy; Scale effect.

## 1. Introduction

The dynamic behaviour of non-standard, curved geometry masonry structures subjected to blast actions is herein studied. A Discrete Element (DE) Method approach is used to account for the intrinsic discrete nature of the masonry. The proposed numerical approach is first validated with

---

*Email addresses:* [filippo.masi@enpc.fr](mailto:filippo.masi@enpc.fr) (Filippo Masi), [ioannis.stefanou@enpc.fr](mailto:ioannis.stefanou@enpc.fr) (Ioannis Stefanou), [victor.maffi-berthier@ingerop.com](mailto:victor.maffi-berthier@ingerop.com) (Victor Maffi-Berthier), [paolo.vannucci@uvsq.fr](mailto:paolo.vannucci@uvsq.fr) (Paolo Vannucci)

recent, well-detailed experimental tests on planar walls and then used to investigate the influence of various micro-mechanical parameters on the response of a circular, barrel vault subjected to an internal explosion. This kind of geometry is particularly interesting due to the interplay between membrane (in-plane) and bending (out-of-plane) modes of deformation and failure.

The motivation of this work is found in the present international context. There is currently a need for better assessing the threat of explosions meant to destroy civil engineering assets. Emblematic monumental brick and stone structures are often primary targets. In the existing, public (non-confidential) literature, neither experimental nor numerical investigations of the response to explosions of typical structural elements of such architectural assets exist. Here we refer to arches, vaults, domes, etc. To this purpose, we propose a detailed numerical approach as a valid tool to analyse the fast-dynamic blast loading response of a typical architectural masonry asset: a barrel vault. This geometry is taken as paradigm in order to better understand the dynamic behaviour of such kind of structures and to identify the dominant parameters that influence their response.

Masonry is a composite material made of discrete building blocks that are quasi-periodically arranged in space. The masonry blocks interact through their interfaces (or joints), where mortar might be present or not (dry masonry). The investigation of the mechanical behaviour of masonry structures attracts significant scientific research, mostly due to the fact that the vast majority of historical buildings and a considerable part of modern constructions are made of masonry. Until now, attention has been focused on the mechanical behaviour of masonry under quasi-static and seismic loads using experimental, numerical, and/or theoretical means, see e.g. [1, 2, 3, 4, 5, 6, 7, 8, 9]. However, less attention is dedicated to their behaviour under explosions, with the exception of flat walls.

We record, for instance, the work of Varma et al. [10] who performed tests on several masonry panels of different thickness subjected to near- and far-field explosions. Gabrielsen et al. [11] experimentally investigated the response to blast loading of full-scale un-reinforced masonry walls with and without development of arching actions (originating in a wall butted against rigid supports and subjected to out-of-plane loads). The strength enhancement of one-way arching masonry walls results from the increase of membrane stresses which gives larger friction forces between adjacent blocks. Dennis et al. [12] conducted experiments on 1/4-scale reinforced masonry walls under blast events. Abou-Zeid et al. [13] studied the response of arching walls made of hollow concrete bricks under several explosive weights, in a far-field scenario. Gagnet et al. [14] performed full-scale explosion tests on masonry walls to investigate the influence of boundary conditions in the development of compressive arching actions within the structure. Keys and Clubley [15] investigated masonry debris distribution and failure patterns of masonry walls when subjected to long duration blast loading. Propagation of cracks was found to occur almost exclusively along the bed joints and damage within the body of individual bricks was negligible. Li et al. [16] investigated through experimental and numerical studies the response of un-reinforced clay brick masonry walls subjected to vented gas explosions. A significant influence of the boundary conditions and wall thickness was found for the mechanical behaviour and the blast performance. More recently, Michaloudis and Gebbeken [17] analysed the response of unreinforced masonry walls constrained to rigid supports and subjected to far-field and contact explosions. The approach of the authors was both experimental and numerical. In the case of far field explosions, global collapse was induced by the failure at the interfaces between blocks and damage of bricks was negligible. To the authors' knowledge, this is the most recent and well-documented experimental work and for this reason will be used as reference for comparison and validation of the proposed model.

It is worth emphasizing that a similar research activity is not reported for non-standard curved

masonry structures, despite the fact that non-planar shapes are common in many monumental structures of high risk (e.g. Gothic cathedrals [18, 19, 20]) and more modern ones ([21, 22]).

As far it concerns numerical modelling of masonry under fast-dynamic excitations, macro-modelling/ continuum approaches dominate in the available literature. Wang et al. [23] developed a predictive method for fragment size and ejection distance of masonry wall under blast loads using a homogenized approach. Wei and Stewart [24] tested the response of masonry walls of different thickness and supporting conditions under far-field blasts with a meso-scale numerical approach. Macorini and Izzuddin [25] performed numerical tests of unreinforced masonry walls through a meso-macro partitioned numerical model. Hashemi Rafsanjani et al. [26] proposed a strain rate dependent anisotropic continuum model for masonry subjected to high rate loading and investigated the influence of tensile strength and wall thickness. Parisi et al. [27] investigated through a finite element macro-model the out-of-plane blast performance of tuff stone masonry walls. Silva et al. [28] developed a homogenized approach accounting for high strain rate effects to analyse masonry panels subjected to impact and blast loads.

Here we develop a DE model for accessing the salient features of the system keeping at minimum modelling assumptions. Our modelling approach takes root in the existing knowledge of the behaviour of planar masonry structures subjected to explosions and extend them to non-standard, curved geometry structures. Blast loads are computed using a dynamic library which accounts for the effect of surface rotation of building blocks as well as the evolution in time of their relative distance with respect to the impinging blast wave. Comparing the available experimental results of Michaloudis and Gebbeken [17] with our numerical model, a very good agreement is found for the evolution of the deflection of the panel and failure. We observe that the mechanical behaviour of the masonry joints plays a leading role in the overall strength and failure of the structure. Failure within the body of masonry bricks does not occur or is usually negligible, as corroborated by experimental tests [13, 15, 17] as well as by theoretical investigations, see e.g. [29] where it is shown that failure of the building blocks is important only under high compression.

Besides the ultimate shear and tensile strength of masonry joints, the dilatancy of interfaces may have an important role on the overall resistance of the structure. Masonry joints show generally no dilatancy, see e.g. [30]. This is in contrast, for instance, with the classical assumption of associativity in the theory of plasticity, which may result in non-conservative predictions of the ultimate load-bearing capacity of masonry structures [6, 7]. Another aspect that seems to influence the overall strength of masonry structures is the size of the building blocks. This inherent scale effect is known to have a direct impact on the dynamics of articulated/blocky masonry structures [31, 32, 33, 34].

Numerical tests are performed to investigate the influence of the above micro-mechanical and geometric parameters on the response of a curvilinear masonry structure, i.e., a circular vault, subjected to surface blasts. A strong dependency of the blast resistance upon dilatancy and friction angle at the interfaces is found, while the mechanical response only slightly depends on cohesion and tensile strength of the mortar joints.

Finally, we investigate the validity of the hypothesis of assuming infinitely rigid masonry blocks. Similarly to what observed for arching masonry walls [27], non-deformable blocks may provide un-realistic predictions of the overall strength of masonry structures. In particular, we prove that a rigid blocks model is affected by a spurious numerical phenomenon, defined here as *rotational locking*.

The paper is structured as follows. In Section 2 we present the Discrete Element model and the main assumptions of our modelling approach. We briefly describe in Section 3 the effects of explosions on targets and the model used to apply the loading on the masonry structure through an external library. Section 4 provides the validation of the proposed discrete model through recent existing experimental results. We perform in Section 5 numerical tests varying several micro-mechanical parameters for a masonry vault under blast loads. Finally, Section 6 explores the appropriateness of a rigid blocks assumption in the DEM simulations.

## 2. Discrete Element Model and modelling assumptions

Herein we rely on the Discrete Element Method to investigate the behaviour of masonry structures subjected to blast loading. The approach allows to directly model several micro-mechanical parameters, such as the geometry of the building blocks and the constitutive behaviour of the interfaces and of the blocks. A discrete approach further allows to simulate the progressive failure of masonry and capture with fidelity the post-peak, softening, dynamic behaviour of a masonry structure with bricks undergoing large displacements and rotations [6, 8, 9, 35]. The DEM simulations are herein carried out using 3DEC software [36]. A central finite differences scheme is used in this code for integrating in time the equations of motion of each block. This code provides the means to apply the conceptual model of a masonry structure as a system of blocks which can be assumed either rigid or deformable. A soft-contact algorithm is used to model the interactions between neighbouring blocks through interfaces/joints.

Herein we model the masonry bricks as deformable blocks interacting through zero thickness contact interfaces, and subdivided into finite-difference meshes of tetrahedral elements. Of course the consideration of deformable blocks increases considerably the calculation time, compared to simulations using infinitely rigid ones. This is why the pertinence of the simplifying assumption of rigid blocks is discussed in Section 6.

In the following, we present the modelling assumptions for the constitutive behaviour of masonry joints and blocks.

### 2.1. Constitutive behaviour of masonry joints

#### 2.1.1. Elastic behaviour

The elastic behaviour of the interfaces is defined through the following stress-displacement relationship [36]:

$$\begin{pmatrix} t_n \\ t_t \end{pmatrix} = \begin{pmatrix} k_n & 0 \\ 0 & k_t \end{pmatrix} \begin{pmatrix} u_n \\ u_t \end{pmatrix}, \quad \text{or} \quad \mathbf{t} = \mathbf{k}^{el} \mathbf{u}, \quad (1)$$

where  $\mathbf{t}$  and  $\mathbf{u}$  are the vectors collecting the normal,  $t_n$ , and tangential,  $t_t$ , forces per joint's unit area and the joint normal,  $u_n$ , and tangential,  $u_t$ , displacement, respectively. The elastic stiffness matrix  $\mathbf{k}^{el}$  collects the normal and tangential stiffness:  $k_n$  and  $k_t$ , respectively.

Normal and tangential stiffness are computed from the properties of the masonry components and the soft-contact assumption. For a deformable block model, the elastic parameters read:

$$k_n = \frac{E_m}{h_m} \quad \text{and} \quad k_t = \frac{G_m}{h_m}, \quad (2)$$

where  $E_m$  and  $G_m$  represent respectively the Young's and shear moduli of mortar and  $h_m$  is the thickness of the masonry joints (for more, we refer to [35]). This expression is considered for both head and bed joints.

### 2.1.2. Plastic and softening behaviour

In the absence of more detailed experimental data regarding the behaviour and the resistance of masonry joints, the Coulomb criterion seems to be a reasonable choice. Several experimental observations (e.g. [1, 37, 38]) justify its use up to moderate compression.

The maximum shear (or tangential) force per joint's unit area  $t_t$  (in N/m<sup>2</sup>) is limited by the Coulomb failure surface:

$$f_1 = t_t - c - t_n \tan \varphi \leq 0, \quad (3)$$

where  $c$  is the cohesion of the interface,  $\varphi$  the friction angle. Compression is here considered negative. In shear/tensional regime a tension cut-off is often used as shown in Figure 1. In other words, the maximum normal force per joint's unit area  $t_n$  (in N/m<sup>2</sup>) is limited by the tensile strength according to:

$$f_2 = t_n - f_t \leq 0, \quad (4)$$

where  $f_t$  is the tensile strength of the interface. The joint forces  $F_t$  and  $F_n$  are related to the corresponding displacements according to

$$F_t = A_j t_t \quad \text{and} \quad F_n = A_j t_n, \quad (5)$$

where  $A_j$  is the joint's area.

The built-in constitutive law presently implemented in 3DEC does not account for joint compressive failure. Although solutions to overcome that issue have been implemented in the existing literature (see e.g. [39]), an infinite compressive strength of the masonry joints is assumed. This hypothesis is *a posteriori* verified by monitoring the compressive stresses in the numerical computations.

The two inequalities (3, 4) define the elastic domain of masonry joints. These surfaces can evolve and contract under combined shear and normal plastic deformation in order to take into account various micro-mechanisms related to progressive softening of the joints. As observed in experimental results on interfaces, a softening behaviour, as depicted in Figure 1, is observed. Accordingly, maximum tensile strength, cohesion, friction angle, and dilatancy,  $\psi$ , can evolve from their initial values  $c$ ;  $f_t$ ;  $\varphi$ ;  $\psi$  to some smaller residual values  $c_{res}$ ;  $f_{t_{res}}$ ;  $\varphi_{res}$ ;  $\psi_{res}$ . All these values can be determined by experimental tests on interfaces. Regarding the plastic flow rule, this is given by the following potentials:

$$g_1 = t_t - t_n \tan \psi, \quad (6)$$

$$g_2 = t_n. \quad (7)$$

If  $\psi = \varphi$  we say that the plastic flow rule is associative (normality condition), otherwise ( $\psi < \varphi$ ) the material obeys a non-associative plastic flow rule. In both cases, the following general relation between the rate of change of forces and the rate of change of total displacements stands:

$$\dot{\mathbf{t}} = \mathbf{k}^{pl} \dot{\mathbf{u}}, \quad (8)$$

with  $\mathbf{k}^{pl}$  the plasticity matrix,

$$\mathbf{k}^{pl} = \frac{k_n}{\kappa + \tan \varphi \tan \psi} \begin{pmatrix} \tan \psi & 1 \\ \tan \varphi \tan \psi & \tan \varphi \end{pmatrix},$$

where  $\kappa = k_n/k_s$ , and  $\dot{\mathbf{t}}$  and  $\dot{\mathbf{u}}$  represent the rate of change of the forces and of the total displacement vectors,  $\mathbf{t}$  and  $\mathbf{u}$ , respectively.

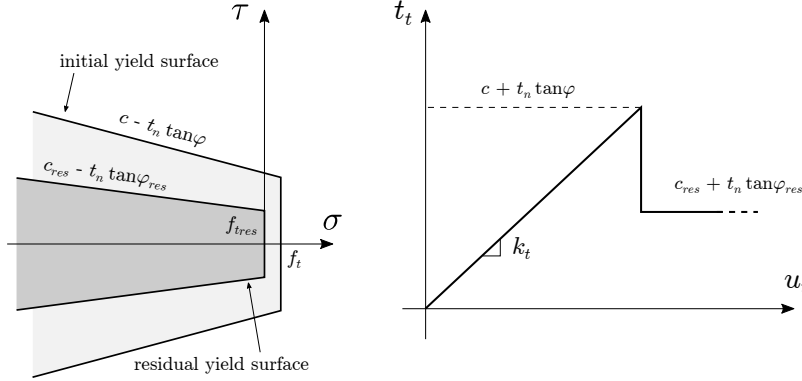


Figure 1: Initial and residual strength surfaces (left) and tangential stress-displacement relationship (right) used for modelling joints behaviour.

## 2.2. Constitutive behaviour of masonry blocks

Blocks are assumed to follow an elastic, isotropic material behaviour. In the DE model, joints have zero thickness, which is not the case in real masonry. For this purpose, the elastic parameters of the blocks have to be modified in order to account for the finite thickness of the joints [35]. Namely, the Young's and shear moduli of the discrete elements become:

$$E_b^* = E_b \left( 1 + \frac{h_m}{h_b} \right) \quad \text{and} \quad G_b^* = G_b \left( 1 + \frac{h_m}{h_b} \right), \quad (9)$$

with  $E_b$  and  $G_m$  being the Young's and shear moduli of the masonry bricks, respectively;  $h_b$  is the height of the masonry bricks;  $h_m$  is the mortar joints' thickness. Notice that the difference between the elastic parameters,  $E_b$  and  $G_m$ , and the corrected ones,  $E_b^*$  and  $G_m^*$ , is very small ( $\approx 5 \div 10$  %) and in general negligible, for typical masonries.

We further assume infinite tensile and compressive strength for the blocks. This may be a strong assumption in the case of near-field explosions and especially in contact detonations, see e.g. [17]. Nevertheless, experimental evidence shows that damage is generally negligible within the body of masonry bricks in moderate to far-field explosions. In these conditions, the collapse of the masonry structure is governed by failure at the interfaces [13, 15, 17]. This is also supported by the fact that the material strength increases at high loading rates, with respect to its quasi-static value. Extensive research showed that at increasing loading rates the resistance of brittle materials increases as well, mainly due to the finite growth rate of micro-cracks [40, 41] and the viscosity of the material [42]. In particular, the dynamic increase factor for tensile strength for geomaterials (such as mortar, tuff, granite, etc.) usually varies between 1 and  $\approx 7$  depending on the developed strain rates, see e.g. [43, 44].

In each computation, stress and strain rates are monitored to verify that the related dynamic strength of the material is such that failure within blocks does not occur. This was true for all simulations presented herein.

### 3. Blast loads

Explosion produces a blast wave of high-pressure accompanying high-temperature and supersonic expansion of gases. The abrupt increase of the pressure carried by a blast wave can produce severe structural damage. When the primary shock meets a target, it generates on it the so-called reflected overpressure,  $P_r$ , which is the difference between the pressure determined by the explosion increased by the reflection at target's surface and the ambient one,  $P_o$ . Figure 2 shows the schematic time variation of  $P_r$ , which is determined by the arrival time of the shock wave,  $t_A$ , the overpressure peak,  $P_{ro}$ , the positive phase duration,  $t_o$ , negative phase duration,  $t_{o-}$ , and the underpressure peak,  $P_{ro-}$ . These parameters are functions of the distance  $R$  and the explosive weight (conventionally expressed in TNT equivalent).

The pressure acting on a target due to blast loading is the algebraic sum of the incident overpressure and the dynamic pressure  $C_D q = \frac{1}{2} \rho u |u|$ , with  $C_D$  the drag coefficient (function of the target shape and Mach and Reynold numbers),  $\rho$  the density, and  $u$  the velocity of gas particles.

The simulation of a blast can be conducted by using different approaches [45, 46]. Herein we refer to empirical models based on experimental results available in the existing literature.

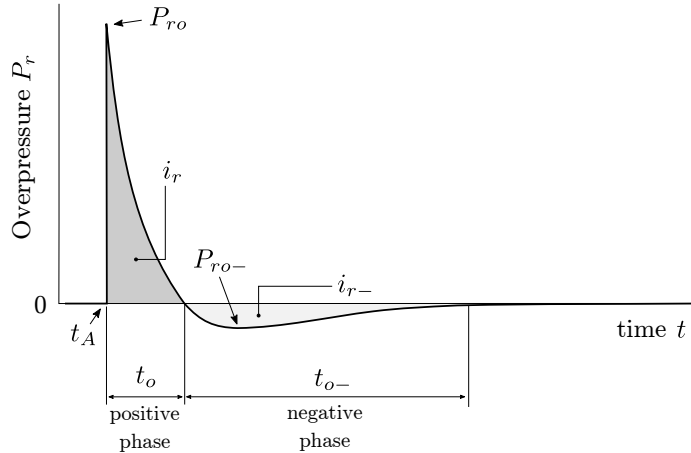


Figure 2: Time evolution of overpressure (i.e. the pressure measured relatively to the atmospheric one) due to an explosion acting on a target.

#### 3.1. Blast model

We model blast actions following the work of Hyde [47] with the empirical model ConWep, which relies on the best-fit interpolations of the experimental results from Kingery and Bulmash [48]. The interpolations allow to determine the blast parameters and pressure loading from the knowledge of the trinitrotoluene (TNT) equivalent explosive weight,  $W$ , and the Hopkinson-Cranz scaled distance,  $Z = R/\sqrt[3]{W}$ . The time evolution of the reflected pressure is modelled with the well established *modified Friedlander equation*,

$$P_r(t) = P_{ro} \left[ \left( 1 - \frac{t}{t_o} \right) \right] \exp \left( -d \frac{t}{t_o} \right), \quad (10)$$

where  $d$  is the exponential decay coefficient. The impulse associated to the positive,  $i_{r+}$ , and the negative phase,  $i_{r-}$ , reads:

$$i_{r+} = \int_0^{t_o} P_{r+} dt = [e^{-d} + d - 1] \frac{P_{ro} t_o}{d^2}, \quad (11)$$

$$i_{r-} = \int_{t_o}^{\infty} P_r dt = -\frac{P_{ro} t_o}{d^2} e^{-d}, \quad (12)$$

respectively. Equation 11 allows to determine the exponential decay coefficient,  $d$ , by equating it with the best-fit interpolation of  $i_{r+}$  from experiments [48].

Blast loads are computed through an external library which accounts for the effects of surface rotation of masonry components due to the pressure load (incident angle effect, variation of the relative distance between blocks and explosive, etc. during incrementation time stepping). Herein the effects due to the angle incidence are modelled with the simplified approach implemented in ConWep [47]. Nevertheless, the external library can treat as well more realistic interpolations and account, in detail, for the effects of the incident angle, see e.g. the approach proposed in [49]. The external library is implemented in C language and Qt widget toolkit is used to realize the dynamic link with the DE Software [36]. Blast loads are applied and updated at each time step with appropriate algorithms (for rigid and deformable blocks) implemented in 3DEC FISH language.

#### 4. Validation of the Discrete Element model

The proposed numerical model is herein compared and validated with existing experimental tests. Among the experiments available in the literature, we select one of the most well-documented [17]. Notice that performing blast experiments either in reduced- or in full-scale presents many difficulties, due to the nature of the loading action, which may result in large uncertainties of the recorded results.

Michaloudis and Gebbeken [17] analysed the response of unreinforced masonry walls subjected to far-field and contact explosions through experimental and numerical investigations. Among four tests, two involved masonry walls which were subjected to the explosion of  $W_1 = 810$  kg and  $W_2 = 1150$  kg of TNT at  $R = 37$  m from the targets. Due to the large stand-off distance, the blast wave impinges almost uniformly and simultaneously the entire target. Nevertheless, no information is given concerning the evolution of the blast pressure in the experimental tests. The brickwork consists of a running bond pattern with bricks of nominal dimensions  $a \times b \times w = 80 \times 240 \times 120$  mm, see Figure 3. The boundaries of the walls are constrained, through mortar interfaces, to stiff fixed supports.

In Test 1 ( $W_1 = 810$  kg,  $R = 37$  m), the observed maximum outward and inward deflection at the centre of the wall are 77 mm and 37 mm, respectively. In Test 2 ( $W_2 = 1150$  kg,  $R = 37$  m), a breach at the centre of the wall originates mainly due to joints failure. Failure within the body of individual bricks is not observed or is negligible [17]. The maximum dimensions of the breach are equal to 4 bricks along the length of the wall and to 13 bricks along the height (see Fig. 6).

In the numerical Discrete Element (DE) model, a constant thickness of the mortar  $h_m = 10$  mm is assumed in the lack of more detailed information for the walls. Table 1 presents the material parameters of the numerical model, which have been selected from the literature, see e.g. [29, 50, 51].

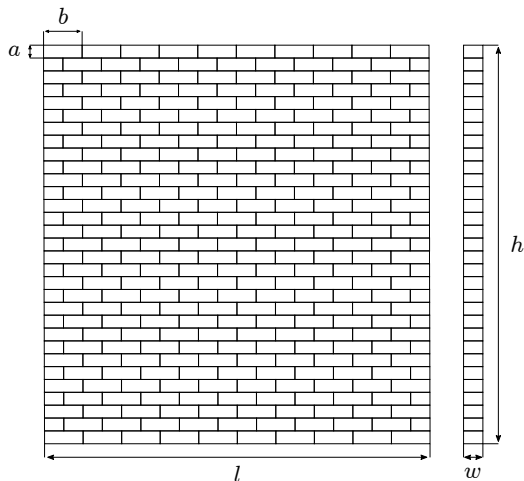


Figure 3: Geometrical model for test 1 and 2 in [17]. The masonry wall has thickness  $w = 120$  mm and running brick bond course. Bricks have nominal size  $a \times b \times w = 80 \times 240 \times 120$  mm.

We recall that subscript *res* identifies the residual (post-softening) value of the parameters (see Fig. 1). In lack of information about the boundary conditions acting on the structure, the wall is considered simply supported at its four edges (only rotations around the supports are allowed), as complete rotational restraint may be difficult to achieve in practice. Blast loads are computed and applied using the dynamic library presented in Section 3.

From convergence analyses for contact and finite difference discretization (see [6, 35]), we find that at least 10 contact points are required to accurately modelling the out-of-plane deflection of the wall under study. Otherwise the numerical results are not reliable. The finite difference mesh for deformable blocks is selected from mesh convergence analyses and consists of tetrahedra with average characteristic length equal to 30 mm [35].

Table 1: Material parameters of the numerical DE model.

Blocks properties			Joints properties					
density	(kg/m <sup>3</sup> )	2470	$k_n$	(GPa/m)	50	$c$	(kPa)	500
$E_b^*$	(MPa)	5220	$k_t$	(GPa/m)	20.83	$f_t$	(kPa)	100
$G_b^*$	(MPa)	2170				$c_{res}, f_{tres}$	(kPa)	0
						$\varphi$	(°)	30
						$\psi$	(°)	0

#### 4.1. Numerical results

We compare in Table 2 the numerical results obtained with the DE model and the test data [17] for Test 1 ( $W_1 = 810$  kg,  $R = 37$  m). The discrete approach agrees remarkably well with the observed maximum outward and inward deflections. It has to be emphasized that typical values for masonry properties were used in the DE model and no fitting was performed. We present in Figure

4 the time evolution of the numerically measured deflection at the centre of the wall. In the free-oscillating response, the system gradually dissipates energy as a result of the slip along interfaces, until equilibrium. A permanent outward deflection of approximately 7.1 mm is measured at the centre.

Table 2: Maximum outward and inward deflection at the centre of the wall for Test 1. Comparison between the observed values and the numerical predictions with the DE model. Typical values for masonry materials were used and no fitting was performed.

Maximum deflection	Experiment	DEM
Outward (mm)	77.0	78.2
Inward (mm)	37.0	38.2

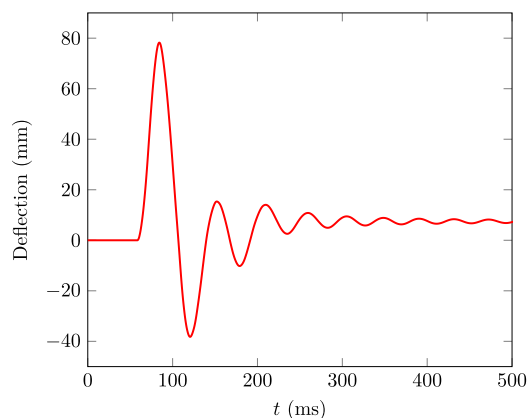


Figure 4: Time evolution of the deflection at the centre of the wall from the numerical DE simulations of Test 1 ( $W_1 = 810$  kg,  $R = 37$  m).

For Test 2 ( $W_2 = 1150$  kg,  $R = 37$  m), we present in Figure 5 the out-of-plane response and the consequent formation of the breach from the numerical simulations. Figure 6 and Table 3 compare the breach dimensions of the numerical simulations with the experimental evidence. The DE model is found to well capture the form of failure and the location of the breach. Nevertheless, a small difference in the number of the bricks that are removed from the wall is observable. This may be due to the complex fluid-structure interaction phenomena that take place during the explosion (and which are not considered in our simulations) and the fact that, in the test, some brick involved in the breach, even being few, break, which is not considered herein.

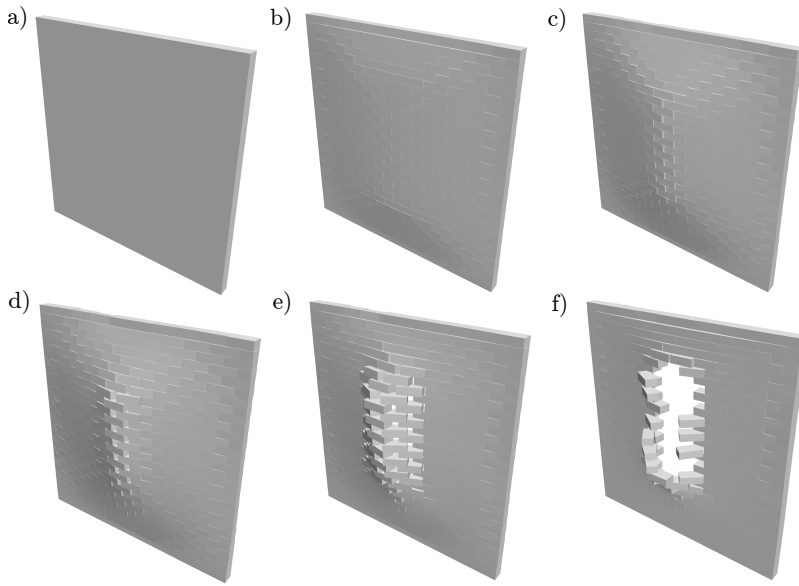


Figure 5: Response of the DE model for Test 2 ( $W_2 = 1150$  kg,  $R = 37$  m), a-e), and final state of the masonry wall, f).

Table 3: Comparison of the breach dimension (height  $\times$  width in terms of number of involved bricks) from the numerical results (DEM) and the experimental test.

Breach	Experiment	DEM
Dimensions	$13 \times 4$	$14 \times 2$
No. involved bricks	40	22

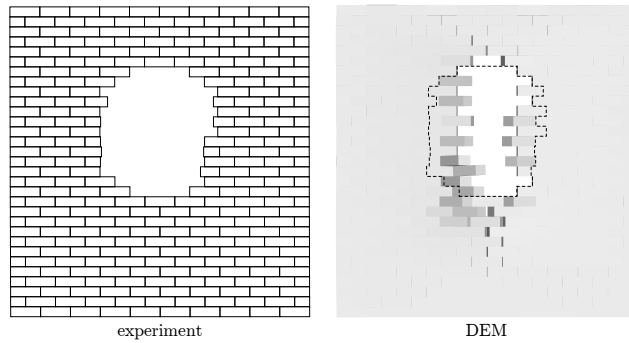


Figure 6: Comparison between the experiment (left) and the numerical DEM results (right) for Test 2 ( $W_2 = 1150$  kg,  $R = 37$  m). The experimental breach extension is schematically represented by the black dashed line. Typical values for masonry materials were used and no fitting was performed. A very good agreement is found.

## 5. Study of the dynamic response of a barrel vault subjected to an internal explosion

Once the proposed model has been validated, we perform numerical tests to investigate the response of a non-standard masonry structure, namely a barrel vault (see Fig. 7), subjected to the action of an internal blast. DEM simulations are used here to understand the influence of various micro-mechanical parameters, such as the dilatancy and the building blocks size, on the dynamic response of the system.

### 5.1. Geometric model and discretization

The geometric model of the considered configuration is presented in Figure 7. The masonry bricks have size  $a \times b \times w = 250 \times 296 \times 200$  mm. The thickness of the mortar is 10 mm. The vault has inner diameter  $d_i = 2800$  mm, thickness  $w$  (outer diameter  $d_e = 3200$  mm), and length  $l = 3060$  mm. The longitudinal length of the structure has been selected upon considerations on the characteristic lengths associated to the blast wave and the hemispherical shock front.

The base ( $y = 0$ ) and the edges ( $z = 0$  and  $z = l$ ) of the structure are assumed to be connected with fixed supports through contact interfaces. The supports have length  $l_s = 150$  mm and thickness  $w$ . They are used to consider the presence of arched ribs, e.g. in a nave.

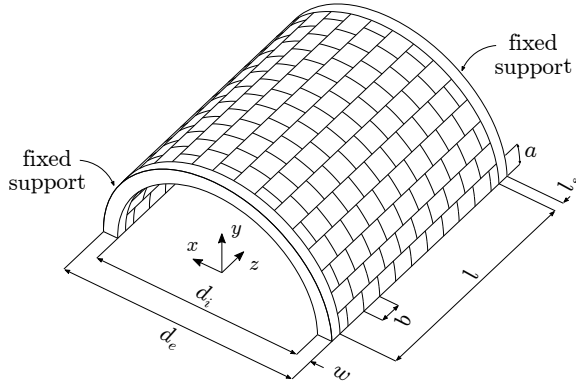


Figure 7: Geometric model of the masonry barrel vault under investigation. Bricks have size  $a \times b \times w = 250 \times 296 \times 200$  mm. The vault has inner diameter  $d_i = 2800$  mm, thickness  $w$  (outer diameter  $d_e = 3200$  mm), and depth  $l = 3060$ . The extremities at  $z = 0$  and  $z = l$ , as well as at the base ( $y = 0$ ) are assumed to be connected to rigid supports through zero thickness interfaces.

The contact discretization for the DE model is studied through two sets of analyses, which are fundamental for assuring reliable numerical results. First, in a quasi-static elastic calculation, the central layer of blocks is subjected to a constant and uniform pressure equal to 100 kPa acting on the inner faces. This allows to determine the fineness of the discretization of contacts along the circumferential and radial directions for each block (mesh convergence analysis). Second, the structure is subjected to the pressure of a surface blast  $W = 10$  kg located at the ground ( $y = 0$ ) and at the centre ( $z = l/2$ ). The deflection of different points at the vault's key is monitored to investigate the influence of the contact discretization along the longitudinal direction ( $z$  axis). On the basis of this mesh convergence analysis, the selected discretization consists of tetrahedra of

average characteristic length equal to 35 mm, with 100 and 36 contact points along the head and bed joints, respectively, see Figure 8.

We present in Figure 9 the deformed shape, along the longitudinal direction, for the selected discretization, obtained at the equilibrium, under a static pressure of 100 kPa.

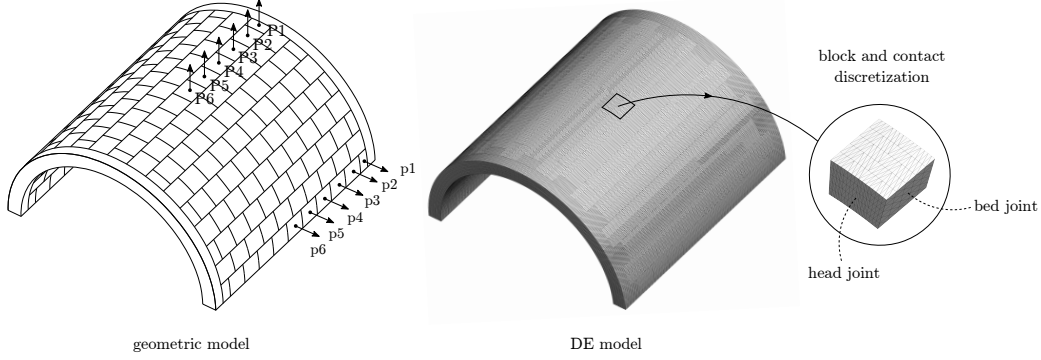


Figure 8: Geometric model of the masonry barrel vault (left), with highlighted monitoring points used in the following simulations, and Discrete Element model with contact discretization and finite difference mesh of the blocks (right).

Once the appropriate discretization is selected, we proceed with the study of the dynamic behaviour of the barrel vault under explosive loads. In the first step, gravity is applied to the structure to reproduce the stress state within the vault under self-weight. The quasi-static equilibrium solution is successively used as the initial state for the simulation of the response to a surface blast due to a TNT explosive weight  $W = 10$  kg, located at the centre ( $y = 0, z = l/2$ ). The elastic parameters for blocks and joints are presented in Table 4. In paragraph 5.2 we investigate the influence of the associativity of the sliding behaviour of masonry joints and the combined effects of friction and dilatancy angles in paragraph 5.3. Different values of cohesion and tensile strength of the interfaces and their dependency on the structural strength of the system are explored in paragraph 5.4. Finally paragraph 5.5 examines the role that the size of the building blocks plays in the dynamic response.

Table 4: Material parameters used in the numerical simulations of the masonry barrel vault.

Blocks properties			Joints properties		
density	( $\text{kg}/\text{m}^3$ )	2000	$k_n$	( $\text{GPa}/\text{m}$ )	100.0
$E_b^*$	( $\text{GPa}$ )	14.5	$k_t$	( $\text{GPa}/\text{m}$ )	41.7
$G_b^*$	( $\text{GPa}$ )	6.0			

### 5.2. The effect of associative or non-associative friction

The influence of the associativity of the masonry joints behaviour is studied, assuming zero cohesion and zero tensile strength for the joints. A constant angle of friction of both the head and

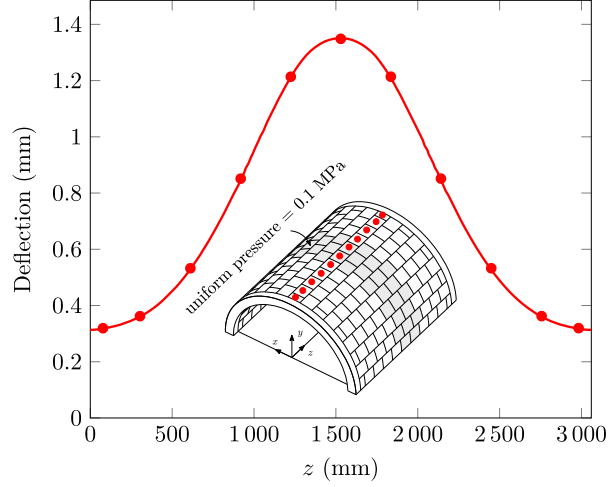


Figure 9: Deformed shape, along the longitudinal direction, at the key’s vault under a constant pressure of 100 kPa applied to the region highlighted in grey. The circles represent the blocks’ centroids. An elastic behaviour is assumed for the masonry joints.

bed joints is considered (cf. 8), namely  $\varphi^b = \varphi^h = 35^\circ$  (superscripts  $b$  and  $h$  refer to bed and head joints, respectively).

Figure 10 presents the time response in terms of the deflection at different points located at the vault’s key (with reference to Fig. 8), assuming an associative sliding behaviour, i.e., equal friction and dilatancy angles,  $\varphi^h = \varphi^b = \psi^b = \psi^h = 35^\circ$ . The blast overpressure, acting on the inner face of the vault, causes an initial outward slip ( $\approx 1$  mm) of the masonry blocks. The elements at the boundaries partially rotate around the rigid supports, while the longitudinal layers of blocks begin to deflect in the outward direction (see Fig. 11). Nevertheless, the relative confinement of the vault (due to the presence of the fixed supports) results in a limited in-plane response. Membrane compressive forces develop in the plane of the vault, along the longitudinal direction, giving rise to so-called *arching actions*. The resulting response of the structure is similar to the one of an arching wall (between supports that restrain the outward movement) subjected to out-of-plane loads [11]. Each layer of bricks along the longitudinal axis develops compressive arching actions (see Fig. 11), while the in-plane response is limited.

When a non-associative behaviour with zero dilatancy is considered, the resistance of the structure is found to decrease, as a consequence of the reduced membrane compressive stress that reduce the apparent friction between the blocks in the longitudinal direction ( $z$  axis). Consequently, the arching mechanism is reduced as well. We present in Figure 12 the displacement history measure at the vault’s key for the case of associative and non-associative (with zero dilatancy) sliding behaviour. The maximum deflection measured in the associative case is found to be 14% smaller than the one obtained with a non-dilatant sliding behaviour, as presented in Tab. 5.2.

As also noticed in [6], joints showing zero dilatancy reduce considerably the stress in masonry. In this case, a non-associative sliding behaviour ( $\psi^b = \psi^h = 0^\circ$ ) results in a reduction of approximately 85 % of both normal and shear stress at the joints and 50% of the maximum principal stress within

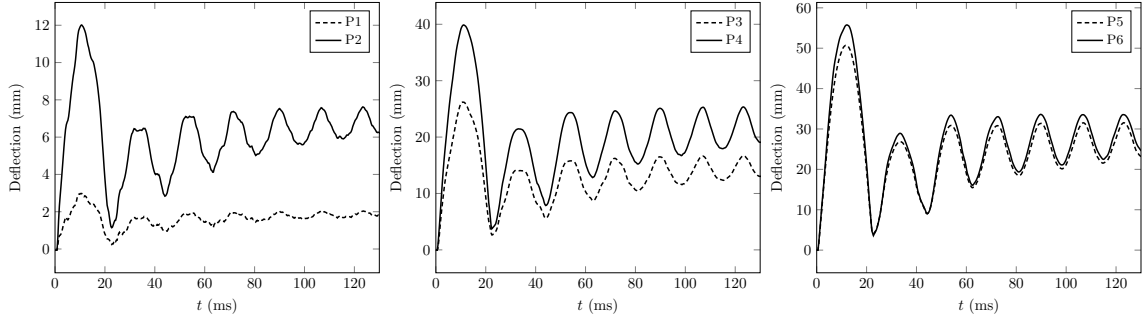


Figure 10: Response of a barrel vault subjected to 10 kg of TNT in terms of the deflection of different points located at the vault’s key (top) and at the base (bottom), see Fig. 8. The results are for  $\varphi^h = \varphi^b = 35^\circ$ ,  $\psi^b = \psi^h = 35^\circ$ ,  $f_t = c = 0$  MPa.

the masonry blocks.

Table 5: Dilatancy  $\psi^b$  and friction angle  $\varphi^h$  considered in the parametric study and related maximum deflection observed in the masonry vault. The results refer to  $\varphi^b = 35^\circ$ ,  $\psi^h = 0^\circ$ , and  $f_t = c = 0$  MPa.

sliding behaviour	$\varphi^b = \varphi^h$ ( $^\circ$ )	$\psi^b = \psi^h$ ( $^\circ$ )	Maximum deflection (mm)
associative	35	35	55.80
non-associative	35	0	65.04

### 5.3. Friction and dilatancy effect for non-associative friction

The effects of a non-associative behaviour, with varying dilatancy, and of the friction angle of the joints are explored. For the bed joints, we consider as follows a constant angle of friction, i.e.,  $\varphi^b = 35^\circ$ , while the dilatancy angle varies between  $0^\circ$  and  $35^\circ$ . At the interfaces representing the head joints, the influence of different values of the friction angle (and zero dilatancy) is explored. The choice originates from the fact that head joints usually are weak planes in masonry structures, due to the lack of the beneficial effect of gravity and construction habits. This stands also for the bed joints whose lying plane makes an angle less than  $90^\circ$  with the direction of applied gravity. Nevertheless, we neglect this latter condition herein. Table 5 presents the considered values of the dilatancy and the friction angle, as well as the maximum deflection numerically measured within the structure.

At varying of the friction angle,  $\varphi^h$ , arching actions still develop, but to a gradually reduced extent, see Fig. 13. As expected, the smaller the friction angle is, the larger the slippage observed between adjacent blocks becomes. This is clearly visible at the supports, point P1 (Fig. 13). In fact, low angle of friction prevents the formation of membrane compressive stress, hence of an effective and beneficial arching mechanism. This is shown in Figure 14 which depicts the response

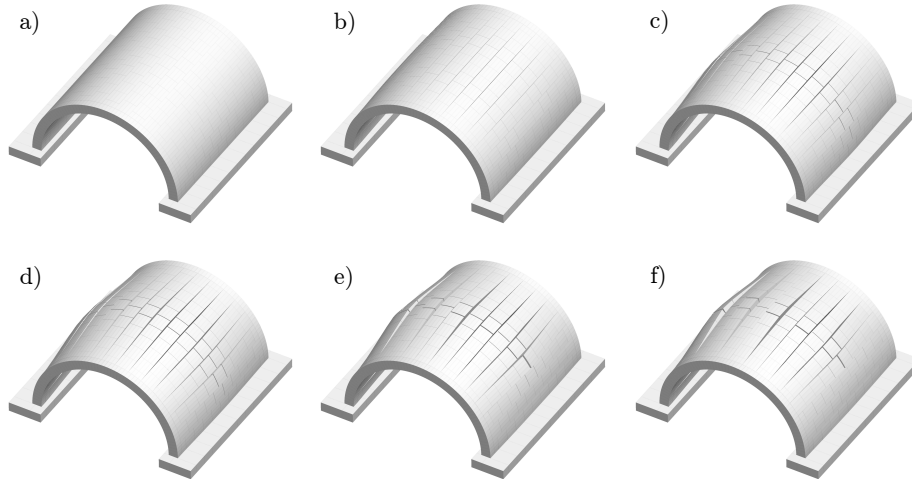


Figure 11: Evolution of response of a barrel vault subjected to 10 kg of TNT and formation of the arching mechanism. The results refer to  $\varphi^h = \varphi^b = 35^\circ$ ,  $\psi^b = \psi^h = 35^\circ$ ,  $f_t = c = 0$  MPa.

and consequent failure of the structure for  $\varphi^h = 10^\circ$ ,  $\varphi^b = 35^\circ$ , and  $\psi^b = \psi^h = 0^\circ$ .

Table 6 and Figure 16 present the maximum deflection observed in the masonry vault for different angles of friction,  $\varphi^h$ , and dilatancy,  $\psi^b$ . Collapse is considered when a maximum deflection equal to 200 mm, i.e., the thickness of the vault, is developed. The response of the system is found to depend only on the friction angle, while the effect of bed joints dilatancy angle on the maximum deflection is negligible. It is worth noticing the presence of a roughly estimated collapse displacement capacity, i.e. the maximum out-of-plane deflection that the system can withstand. This can be clearly seen for the case with  $\psi = 0^\circ$ , for which the effects of the friction angle  $\varphi^h$  are widely investigated. For angles  $\varphi^h \geq 15^\circ$ , the numerically measured maximum deflection remains almost constant,  $u_{max} \approx 60$  mm. For  $\varphi^h = 10^\circ$ , the displacement increases by 20 %, i.e.  $u_{max} = 87$  mm, and collapse occurs at smaller angles of friction. The definition of a collapse displacement capacity is usually applied to out-of-plane load bearing walls and it can be roughly estimated as half of the wall thickness,  $u_{max} \approx w/2$ , see e.g. [52] and [27]. The numerical results for the barrel vault (Fig. 16) seem to corroborate that the same stands for a more complex structure, i.e.,  $u_{max} \approx w/2 \approx 100$  m.

Figure 15 displays the time-evolution of the out-of-plane displacement in function of the dilatancy angle of the bed joints,  $\psi^b$ , and for constant friction angles  $\varphi^b = 35^\circ$  and  $\varphi^h = 10^\circ$ . We clearly notice that the first-peak deflection is invariant of the joints dilatancy. Nevertheless, the dynamic response, i.e. the evolution in time of the deflection, slightly depends on the dilatant behaviour of the joints. In particular, an increase of the post-peak deflection is observed for higher dilatancy. Indeed, the larger the dilatancy of the interfaces is, the higher the transmitted compressive thrust is and the lower the sliding becomes.

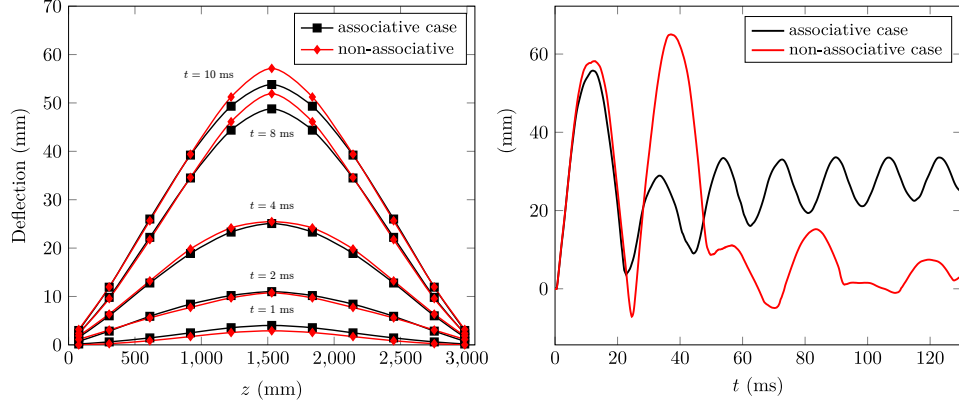


Figure 12: Response of a barrel vault subjected to 10 kg of TNT in terms of the deformed shape at vault’s key (left) and deflection at point P6 (right), for a dilatant behaviour of the masonry joints and assuming a non-associative sliding behaviour ( $\psi^b = \psi^h = 0^\circ$ ). The results are for  $\varphi^h = \varphi^b = 35^\circ$ ,  $f_t = c = 0$  MPa.

#### 5.4. Cohesion and tensile strength effect

The effect of the cohesion and tensile strength of the bed joints is herein investigated considering  $\varphi^b = 35^\circ$  and  $\varphi^h = 10^\circ, 5^\circ$ , and zero dilatancy  $\psi^b = \psi^h = 0^\circ$ . The case with  $\varphi^h = 10^\circ$  is selected in order to investigate the effects on the dynamic response. Indeed, for the same value of the friction angle and zero cohesion and tensile strength, the vault does not undergo collapse (cf. Tab. 5.3). The influence of the two strength parameters on the failure mode and collapse capacity of the structure is instead investigated for  $\varphi^h = 5^\circ$  (collapse for  $f_t = c = 0$  MPa, cf. Tab. 5.3). The selected combinations of values for cohesion and tensile strength are presented in Table 7. Once the onset of tensile and/or shear failure is reached, the residual values of cohesion and tensile strength are imposed to be zero (see Fig. 1). Zero cohesion and zero tensile strength are assumed for the head joints.

Figure 17 shows the response of the system for  $\varphi^h = 10^\circ$  and a wide range of the value of the strength parameters. We notice that both cohesion and tensile strength do not influence the first-peak response of the structure. Only the post-peak response slightly depends on the two parameters, due to the increased/reduced amount of the number of joints that underwent softening. This holds true since the dynamic response is strongly influenced by the relative slip that takes place at the head joints along the longitudinal direction ( $z$  axis), for which zero cohesion and tensile strength are always assumed.

In the case of  $\varphi^h = 5^\circ$ , the system’s failure mode and collapse capacity are found to be independent from the value of tensile strength and cohesion, see Tab. 5.4. In particular, the vault is found to collapse with the same mode depicted in Figure 14, independently of the choice of  $f_t$  and  $c$ . The same was found also for different values of the dilatancy.

Table 6: Dilatancy  $\psi^b$  and friction angle  $\varphi^h$  considered in the parametric study and related maximum deflection observed in the masonry vault. The results refer to  $\varphi^b = 35^\circ$ ,  $\psi^h = 0^\circ$ , and  $f_t = c = 0$  MPa.

$\psi^b$	$\varphi^h$	Maximum deflection (mm)	$\psi^b$	$\varphi^h$	Maximum deflection (mm)
( $^\circ$ )	( $^\circ$ )	(mm)	( $^\circ$ )	( $^\circ$ )	(mm)
0	35	65.04	2	10	86.71
	20	63.45		5	> 200
	15	66.24		0	> 200
	10	86.86			
	5	> 200			
	0	> 200			
5	10	86.66	10	10	86.57
	5	>200		5	>200
	0	>200		0	>200

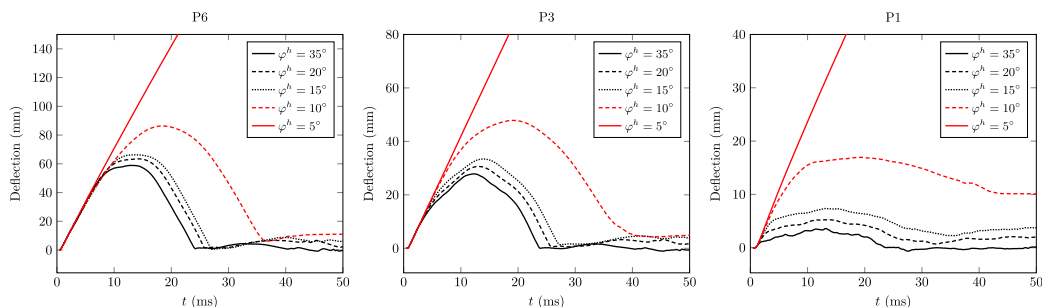


Figure 13: Influence of the head joints angle of friction,  $\varphi^h$ , on the dynamic response of a barrel vault subjected to 10 kg of TNT in terms of the deflection of different points (P6, P3, and P1 cf. Fig. 8). The results refer to  $\varphi^b = 35^\circ$ ,  $\psi^b = \psi^h = 0^\circ$ , and  $f_t = c = 0$  MPa.

### 5.5. Building blocks size effect

The size of the building blocks can influence the compression and the shear strength of the structure, as well as its stiffness [53] and inertia [34]. Several are the reasons of the scale effects of the building blocks. Among those, the number of joints in the structure is usually the leading parameter that influences the dynamic response, energy dissipation due to friction, and overall strength.

Numerical analyses for a selection of material parameters from the previous parametric studies are herein performed to highlight the building blocks scale effect. More precisely, we investigate the associative and non-associative behaviour of masonry joints by varying the blocks size.

The resistance of the vault is studied using blocks that are half and twice their original size, assuming constant overall thickness  $w = 200$  mm (see Fig. 18) and mortar height  $h_m = 10$  mm.

Table 8 and Figure 19 present the maximum deflection that was reported within the vault for

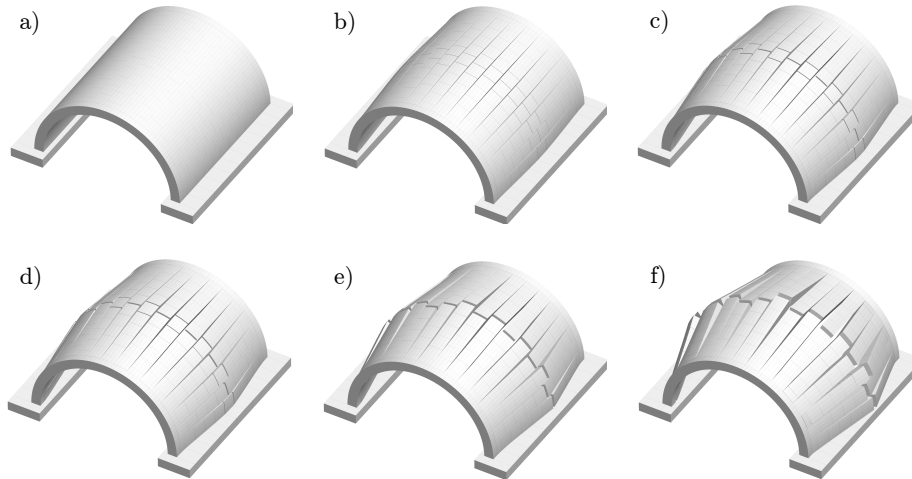


Figure 14: Evolution of response of a barrel vault subjected to 10 kg of TNT. The results are for  $\varphi^b = 35^\circ$ ,  $\varphi^h = 10^\circ$ ,  $\psi^b = \psi^h = 0^\circ$ ,  $f_t = c = 0$  MPa.

different values of the dilatancy and friction angles and highlight the importance of the horizontal joints.

The system with half the blocks size displays an increase in the overall outward deflection of the structure due to the larger number of interfaces in the system. It is worth noticing that the mortar thickness is assumed to be the same in each model, thus the normal and tangential stiffness,  $k_n$  and  $k_t$ , are kept the same between the models, cf. Eq. (2). Therefore, the larger number of masonry joints results in a decrease of the overall flexural stiffness of the structure.

Similarly to what observed in paragraph 5.2, masonry joints with zero dilatancy result in an increased out-of-plane response also for blocks that are half the reference size (the maximum deflection is 9% larger than the one related to the associative case). Moreover, the zero dilatancy joints display reduced stress (90 % of compressive stress and 92 % of shear stress) with respect to the associative case.

The model with twice the blocks size displays smaller out-of-plane displacement and reduced bending, if compared to the reference blocks size, for the case  $\varphi^b = \varphi^h = 35^\circ$ . The reason lies on the same consideration made for the half blocks size: larger blocks result in higher flexural stiffness. Figure 20 displays the dynamic response for different building blocks sizes assuming (a) an associative sliding behaviour and (b) zero dilatancy masonry joints. Also in the case of double blocks size, the non-associative sliding behaviour corresponds to increased out-of-plane displacements (the maximum deflection is found to be 12% larger than the associative case) and reduced stress in the masonry (namely, the compressive stresses are reduced to the 96 % while the shear stress to the 95 % of the ones corresponding to an associative behaviour).

For  $\varphi^b = 35^\circ$  and  $\varphi^h = 10^\circ$  (see Tab. 5.5), we find that the model with double blocks size displays larger deflections, with respect to the reference size. Indeed, an increase in the blocks dimensions corresponds to a decrease of the number of masonry joints, which further gives smaller overall plastic dissipation, namely friction work, and larger relative slippage. In particular, the total friction work with double blocks size is approximately 50% smaller than the one corresponding to

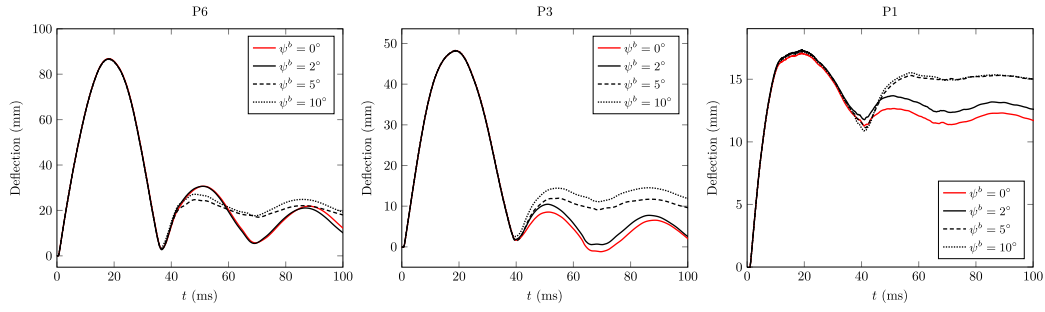


Figure 15: Influence of the bed joints dilatancy,  $\psi^b$ , on the dynamic response of a barrel vault subjected to 10 kg of TNT in terms of the deflection of different points (P6, P3, and P1 cf. Fig. 8). The results refer to  $\varphi^b = 35^\circ$ ,  $\varphi^h = 10^\circ$ ,  $\psi^h = 0^\circ$ , and  $f_t = c = 0$  MPa.

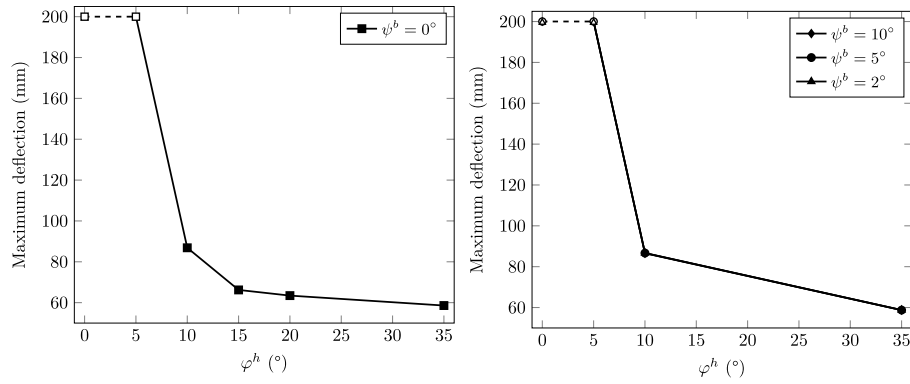


Figure 16: Maximum deflection observed in the masonry vault at varying of  $\varphi^h$  and  $\psi^b$  ( $\varphi^b = 35^\circ$ ,  $\psi^h = 0^\circ$ ,  $f_t = c = 0$  MPa.). High friction angles improve the resistance of the structure through dissipation at the joint interfaces.

the model with half blocks size, see Fig. 21.

Table 7: Cohesion  $c$  and tensile strength  $f_t$  considered in the parametric study and related maximum deflection observed in the masonry vault for  $\varphi^b = 35^\circ$ ,  $\psi^b = \psi^h = 0^\circ$ . The residual values are kept constant  $c_{res} = f_{t\,res} = 0$  MPa.

$f_t$ (MPa)	$c$ (MPa)	Maximum deflection	
		$\varphi = 5^\circ$ (mm)	$\varphi = 10^\circ$ (mm)
0	0	> 200	86.86
	0.1	> 200	86.57
	0.5	> 200	86.55
0.1	0.5	> 200	86.29
0.5	1.5	> 200	
1.5	3.0	> 200	

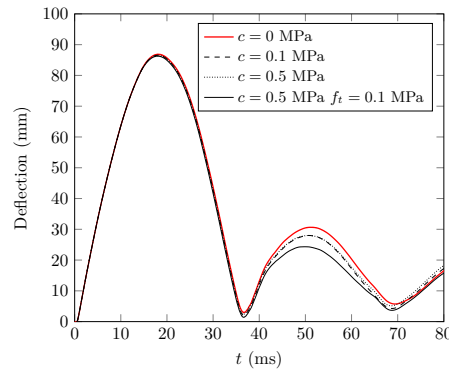


Figure 17: Time evolution of the deflection at the centre of the vault's key (deformable blocks) for different combinations of cohesion and tensile strength of the interfaces. The parameters are found to have small influence on the overall out-of-plane response of the structure.

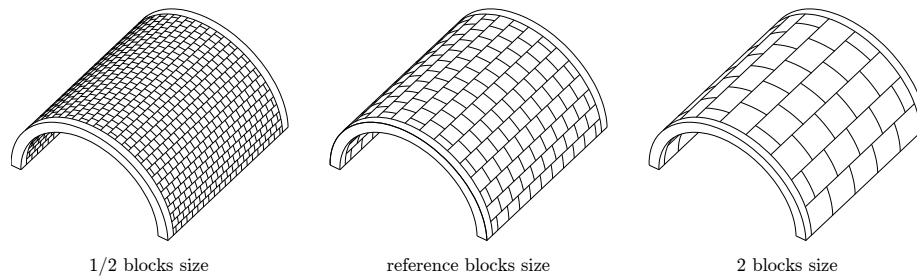


Figure 18: The building blocks size effect is investigated using blocks that are half and twice their original size, assuming constant overall thickness  $w = 200$  mm and mortar height  $h_m = 10$  mm.

Table 8: Building blocks size effect on the maximum deflection observed within the structure. The results refer to  $f_t = c = 0$  MPa.

$\varphi^b$	$\varphi^h$	$\psi^b$	$\psi^h$	Maximum deflection		
				1/2 blocks size (mm)	reference blocks size (mm)	2 blocks size (mm)
35	35	35	35	64.55	55.80	52.08
				70.95	65.04	59.29
35	10	10	0	121.95	53.62	71.51
				126.97	86.86	71.55

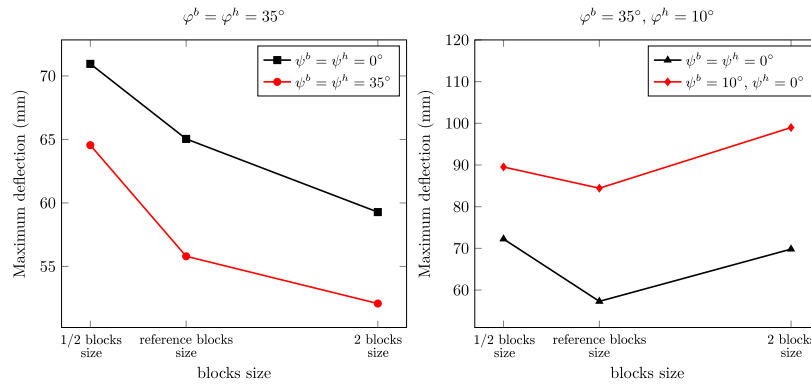


Figure 19: Comparison of the maximum deflection observed in the masonry vault for different size of the building blocks, with  $\varphi^b = \varphi^h = 35^\circ$  (left) and  $\varphi^b = 35^\circ$ ,  $\varphi^h = 10^\circ$  (right). The results are for  $f_t = c = 0$  MPa.

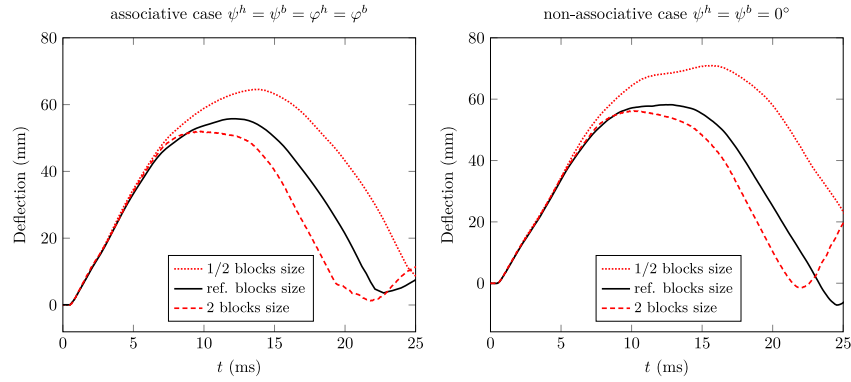


Figure 20: Comparison of the response of the masonry vault in terms of deflection at the centre of the vault's key (right, P6, cf. 7) for different size of the building blocks. The results are for  $\varphi^b = \varphi^h = 35^\circ$  and  $f_t = c = 0$  MPa.

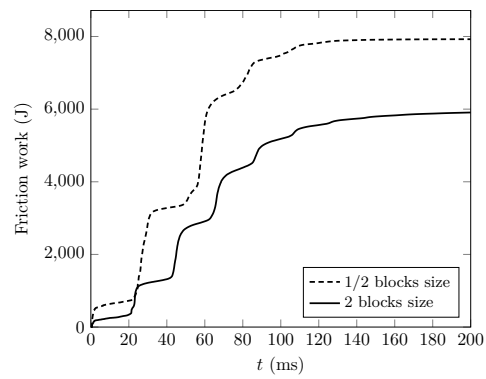


Figure 21: Masonry joints friction work for the structure with half and double blocks size. The results are for  $\varphi^b = \varphi^h = 35^\circ$ ,  $\psi^b = \psi^h = 0^\circ$ , and  $f_t = c = 0$  MPa.

## 6. Rigid vs deformable blocks. Is a rigid blocks assumption pertinent?

Herein we investigate the simplified modelling assumption of infinitely rigid blocks which is often preferred in the literature, see e.g. [54, 55, 56, 6], because of its reduced computational cost with respect to the more detailed model with deformable blocks we are using herein. Under in-plane conditions, the rigid blocks assumption is usually reasonable under relatively low compressive loads, where the deformation is principally concentrated at the interfaces [3]. Moreover, from an energy point of view, the assumption of rigid blocks is supposed to provide safer estimations (lower bound) of the overall strength. Nevertheless, for masonry structures subjected to out-of-plane loading, like those due to a blast, a rigid blocks model may give unrealistic results, see e.g. [27, 35].

In a previous research [35], we proved that the rigid blocks model may display unrealistic rotational (inter-)locking between adjacent blocks under out-of-plane blast loading of planar walls [17]. Here attention is focused on the influence of the blocks deformability for a more complex geometric structure; the barrel vault analysed in the previous Section.

As mentioned in Section 5, several contact points through the thickness of the masonry structure undergoing out-of-plane displacement are required both for rigid and deformable blocks models (see also [57, 58, 6, 35]). However, in a rigid block model, the stress distribution at the interfaces is linear.

Consequently, an accurate discretization of contacts is fundamental. For instance, it has been proved that in the frame of the DEM code herein used, 3DEC, at least 3 contact points along the thickness are required to obtain a satisfactory representation of the bending stiffness [58].

With rigid blocks, the normal and tangential stiffness ( $k_n$  and  $k_t$ , respectively) of the interfaces are appropriately modified with respect to the expressions previously derived (see Sect. 2) in order to account for the deformability of the blocks in the real structure (see also [39]):

$$k_n = \frac{E_b E_m}{E_b h_m + E_m h_b}, \quad (13)$$

$$k_t = \frac{G_b G_m}{G_b h_m + G_m h_b}. \quad (14)$$

This expression is considered for both head and bed joints. In the former case, the block thickness  $h_b$  represents the brick length, while in the latter one,  $h_b$  is the brick height.

Table 9 displays the material elastic parameters used for the model with rigid blocks, derived from those given in Table 4 (for deformable DE) and considering the non-deformability of the blocks, see Eq.s (13, 14). The material parameters that define the plasticity behaviour and the corresponding softening remained unchanged, see Sect. 2. The fineness of the contacts discretization is investigated following the same approach used for deformable blocks (see Sect. 5, paragraph 5.1). The selected discretization consists of 20 contact points at each masonry joint (disposed in an approximate grid of  $4 \times 5$ ).

The numerical assumption of infinitely rigid masonry blocks is investigated through comparisons of the results obtained with the deformable blocks model presented in Sections 4 and 5). First, the non-deformability of blocks is explored under quasi-static conditions, applying a constant pressure to a portion of the vault, as in paragraph 5.1. Second, the dynamic response to blast loading is

Table 9: Material parameters used in the numerical simulations of the masonry barrel vault using a rigid block model. Superscripts  $b$  and  $h$  refer to bed and head masonry joints, respectively.

Blocks properties			Joints properties					
density	(kg/m <sup>3</sup> )	2000	$k_n^b$	(GPa/m)	36.0	$k_n^h$	(GPa/m)	32.0
			$k_t^b$	(GPa/m)	15.0	$k_t^h$	(GPa/m)	13.4

studied.

### 6.1. Rigid vs deformable blocks under quasi-static conditions

A constant uniform pressure equal to 100 kPa is applied to a central layer of the barrel vault (see Fig. 9). We assume a linear elastic behaviour of the interfaces for both models as in the case with deformable blocks (par. 5.1).

Figure 22 displays the deformed shape obtained at the equilibrium, using rigid and deformable blocks, respectively. The rigid discrete model shows higher bending stiffness due to what we define

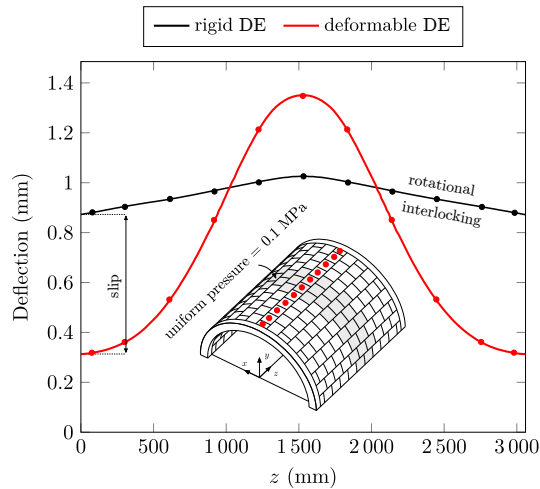


Figure 22: Comparison of the discrete element model with deformable and rigid blocks under a constant pressure 100 kPa applied to the region highlighted in grey. An elastic behaviour is assumed for the masonry joints.

herein as *rotational locking*; a spurious numerical effect leading to a stiffer response in bending as shear locking does in the Finite Element Method. The rotational locking is an artefact that stems from the modelling assumptions of infinitely rigid blocks and of representing masonry interfaces (in the DEM here used, 3DEC [36]) by only two elastic parameters, namely a normal and a tangential stiffness, which leads to a stiffer response.

In the case of the barrel vault subjected to a quasi-static load, the deformed shape with rigid blocks hence consists mostly in a outward slip, as clearly shown in Figures 22 and 23, where a representative scheme of the rotational locking phenomenon is schematically presented.

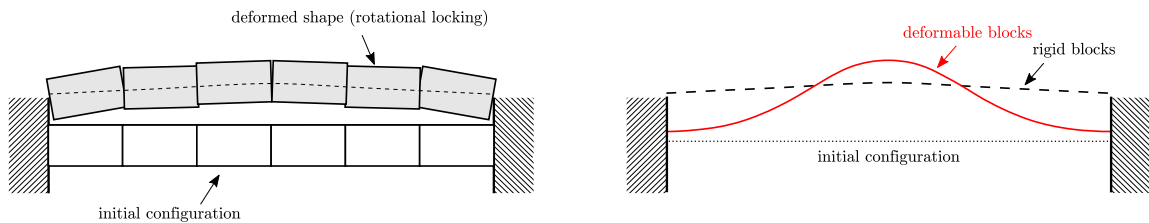


Figure 23: Representative scheme of the rotational locking displayed by infinitely rigid blocks (left) and comparison of the resulting deformed shaped with a deformable blocks model (right).

## 6.2. Rigid vs deformable blocks under blast actions

We explore here if the modelling assumption of rigid blocks is pertinent under fast-dynamic excitations, namely blast actions. We assume zero cohesion and tensile strength,  $f_t = c = 0$  MPa, constant angle of friction of the joints,  $\varphi^b = \varphi^h = 35^\circ$ , and either an associative sliding behaviour ( $\psi^b = \psi^h = \varphi^b = \varphi^h$ ) or zero dilatancy joints,  $\psi^b = \psi^h = 0^\circ$ .

In Figure 24 we compare the evolution of the deformed shape for both rigid and deformable blocks models subjected to 10 kg of TNT. When an associative behaviour of the interfaces is assumed, the overall response predicted by rigid DE agrees well with the one obtained with deformable ones. The relative error is smaller than 2.7%, see Table 10.

However, if a more realistic sliding behaviour of the masonry joints is assumed (i.e., zero dilatancy), the rigid blocks model response is found to highly differ from the one predicted by the deformable DE model. Rotational locking limits the bending response, hence the central (rigid) block, at the vault's key, slips over the adjacent brick (see Fig. 24). This ultimately leads to the loss of any arching mechanism (differently to what observed with deformable blocks). The lack of confinement along the longitudinal direction results in a large slippage at the boundaries. For the non-associative case, the error of rigid blocks associated to the maximum deflection is almost 30%.

Table 10: Maximum deflection observed in the masonry vault at varying of  $\varphi^h$  and  $\psi^b$  ( $\varphi^b = 35^\circ$ ,  $\psi^h = 0^\circ$ , and  $f_t = c = 0$  MPa). Comparison between the numerical results obtained with infinitely rigid blocks and deformable ones.

sliding behaviour	$\varphi^b = \varphi^h$	$\psi^b = \psi^h$	Maximum deflection		
			deformable blocks (mm)	rigid blocks (mm)	rigid to def. blocks error (%)
	( $^\circ$ )	( $^\circ$ )			
associative	35	35	55.80	57.29	2.67
non-associative	35	0	65.04	84.43	29.8

### 6.2.1. Influence of the building blocks size

We explore the influence of the building blocks size on the phenomenon of rotational locking affecting the numerical rigid blocks computations. This is accomplished with numerical simulations with the previous choice of material parameters (see paragraph 6.2), using blocks that are half and

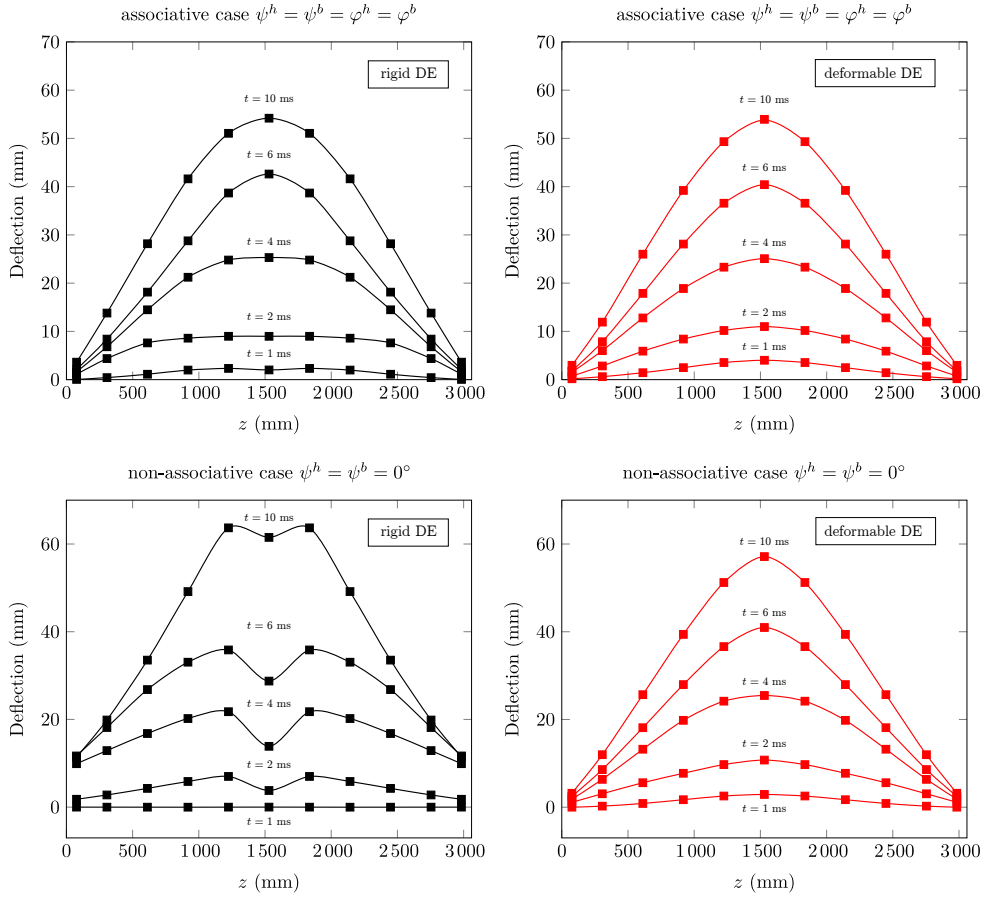


Figure 24: Final state of the masonry vault obtained with deformable blocks (left) and rigid ones (right). The results are for  $\varphi^h = 35^\circ$ ,  $\varphi^b = 10^\circ$ ,  $\psi^b = 5^\circ$ ,  $\psi^h = 0^\circ$ , and  $f_t = c = 0$  MPa.

twice their original size, assuming a constant overall thickness  $w = 200$  mm (see Fig. 18, paragraph 5.5).

Table 11 presents the maximum deflection measured within the structure for friction angle  $\varphi^b = \varphi^h = 35^\circ$ . The results obtained with infinitely rigid blocks and their relative error are also shown.

We find that the rotational locking phenomenon influences the rigid blocks model, independently from the size of the building blocks. Nevertheless, major differences between deformable and rigid blocks are found for bricks of twice the original size. The associativity or not of the sliding behaviour of the masonry joints is, once again, found to affect the rigid model predictions, even if to a smaller extent with respect to the reference block size.

The simplified assumption of rigid blocks is thus found to be not suitable for both quasi-static and fast-dynamic loads (independently from the size of building blocks).

Table 11: Maximum deflection observed in the masonry vault at varying of the building blocks size. Comparison between deformable and rigid blocks models, and corresponding relative error, between parentheses. The results are for  $c = f_t = 0$  MPa.

sliding behaviour	blocks	$\varphi^b = \varphi^h$ (°)	$\psi^b = \psi^h$ (°)	Maximum deflection		
				1/2 blocks size (mm)	reference blocks size (mm)	2 blocks size (mm)
associative	deformable	35	35	64.55	55.80	52.08
	rigid			72.25 (11.93 %)		
non-associative	deformable	35	0	70.95	65.04	59.29
	rigid			89.52 (26.17 %)		

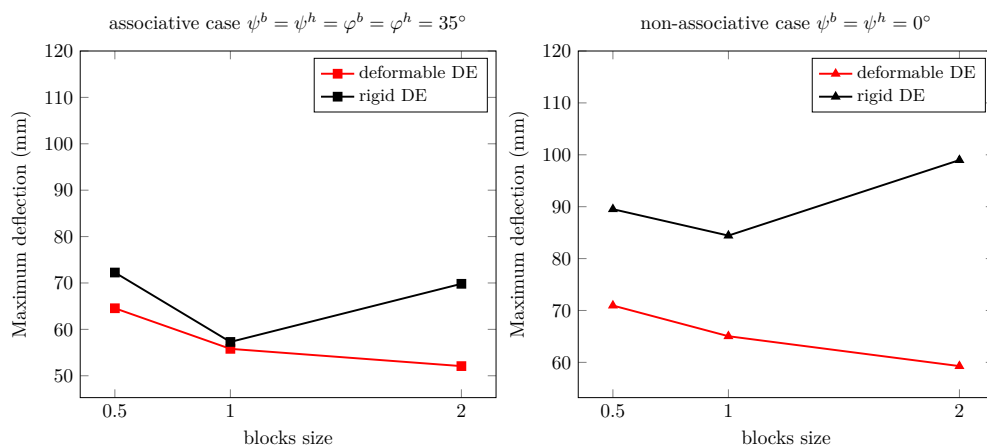


Figure 25: Comparison of the response of the masonry vault in terms of deflection in the proximity of fixed supports (left) and at the centre of the vault's key (right) for different size of the building blocks. The results are for  $\varphi^h = 10^\circ$ ,  $\psi^b = 0^\circ$ , and  $c = f_t = 0$  MPa.

## 7. Concluding remarks

The dynamic behaviour of masonry structures subjected to blast actions was studied here. For this purpose, a numerical model based on DEM was presented and validated on the basis of recent existing, detailed experimental tests involving planar masonry structures subjected to far-field explosions. A very good agreement of the mechanical response and of the failure mode was found between the numerical results and the experimental ones.

Once the numerical model was validated, it was used to assess the response of a curved masonry element, a barrel vault, to an internal blast, for which experimental data are not available. This kind of structures are of particular interest due to the interplay between membrane (in-plane) and bending (out-of-plane) modes of deformation and failure. The mechanical behaviour and out-of-plane response were investigated through detailed parametric studies in order to assess the most

dominant parameters. Here we examined the influence of micro-mechanical parameters such as the joints' dilatancy and friction angle, the cohesion and tensile strength of the mortar joints, as well as the size of the building blocks. Typical values or range of values for masonry were considered for the above mentioned parameters.

For the numerical examples that were investigated, it was shown that the response of a barrel vault restrained to fixed supports is similar to that of a planar wall subjected to out-of-plane loads, butted against rigid supports. Under the action of blast loads, membrane compressive forces develop and the longitudinal layers of brick bend, giving rise to an arching mechanism.

As a result, masonry joints with zero dilatancy (non-associative plastic behaviour) lead to a considerable reduction of the membrane compressive stresses, hence to a reduction of the friction between the blocks, and consequently to an increase of the out-of-plane displacements. In particular, the maximum outward deflection is found to be 14 % larger with respect to the associative case, where  $\psi = \varphi$ . Moreover, we showed that zero dilatancy of joints decreases the stress in the masonry ( $\approx 85$  % within the interfaces and  $\approx 50$  % within the blocks). This is not a surprising result but its quantification through our analyses shows the importance of non-associativity in the investigation, modelling, and design of masonry structures. This limits the application of conventional analysis tools of plasticity theory, such as limit analysis. Therefore dilatancy is related to two competing mechanisms, one that enhances failure due to sliding at the joints, when dilatancy is low, and another that enhances brick failure when dilatancy is high. These competing effects give the possibility to design mortars providing optimal dilatancy for a given structural system.

On the contrary, cohesion and tensile strength of the masonry joints are found to have negligible influence on the maximum deflection, at least for the typical values tested herein ( $0 \div 1.5$  MPa for tensile strength and  $0 \div 3$  MPa for cohesion). As far it concerns the effect of the size of the blocks, it was found that in general the larger the blocks are, the higher the strength of the masonry becomes, see also [34, 6, 53].

Scaling arguments and numerical simulations showed that the high loading rate effects on the material strength are almost negligible for the structure under study. Indeed, in all of the computations, strain rates were found to be lower than  $2 \text{ s}^{-1}$ . Hence the beneficial effects of high loading rates on the strength of the materials are limited. Moreover, the above mentioned negligible influence of cohesion and tensile strength on the dynamic response of the masonry vault shows that taking into account the high rates phenomena at the material level is unimportant for the investigated system.

It is worth emphasizing that, despite the very good agreement with the experimental results for the planar case, the fineness of the predictions for the curved structure has increased calculation cost. A common strategy in DEM analyses for reducing this cost is to consider rigid blocks instead of deformable ones. However, such an assumption may have considerable effects on the structural response when a certain degree of confinement takes place, which is also our case. This is why the assumption of infinitely rigid blocks was also investigated by comparing the numerical results obtained using deformable blocks. In general, the discrete model with rigid blocks showed higher bending stiffness due to *rotational locking*. Rotational locking is a spurious (artificial) increase in stiffness of the DE model which leads to an underestimation of the deflections of the order of  $\approx 3 \div 67\%$  of the results obtained with a deformable block model. As a result, rigid blocks give unsatisfactory predictions for both the quasi-static and dynamic response of the system.

The results obtained in this paper can be useful for improving our understanding on the dynamic behaviour of masonry structures under blast actions, for which the scientific literature is limited. Moreover, it gives useful insight and can be used as benchmark to corroborate numerical approaches based on continuum mechanics (upscaling/homogenization) before being applied for the study of large masonry structures of non-standard geometry, for which the DEM is prohibitive due to the high computational cost.

## References

- [1] R. van der Pluijm, Out-of-Plane bending of Masonry. Behavior and Strength, Technische Universiteit Eindhoven, 1999.
- [2] P. B. Lourenço, Computational strategies for masonry structures., TU Delft, The Netherlands.
- [3] I. Stefanou, K. Sab, J.-V. Heck, Three dimensional homogenization of masonry structures with building blocks of finite strength: A closed form strength domain, *International Journal of Solids and Structures* 54 (2015) 258–270.
- [4] I. Stefanou, I. Psycharis, I.-O. Georgopoulos, Dynamic response of reinforced masonry columns in classical monuments, *Construction and Building Materials* 25 (12) (2011) 4325 – 4337. doi:<https://doi.org/10.1016/j.conbuildmat.2010.12.042>.
- [5] M. Godio, I. Stefanou, K. Sab, J. Sulem, S. Sakji, [A limit analysis approach based on cosserat continuum for the evaluation of the in-plane strength of discrete media: Application to masonry](#), *European Journal of Mechanics - A/Solids* 66 (2017) 168 – 192. doi:<https://doi.org/10.1016/j.euromechsol.2017.06.011>. URL <http://www.sciencedirect.com/science/article/pii/S0997753816304727>
- [6] M. Godio, I. Stefanou, K. Sab, Effects of the dilatancy of joints and of the size of the building blocks on the mechanical behavior of masonry structures, *Meccanica* 53 (7) (2018) 1629–1643. doi:[10.1007/s11012-017-0688-z](https://doi.org/10.1007/s11012-017-0688-z).
- [7] L. Cascini, R. Gagliardo, F. Portioli, LiABlock\_3D: A Software Tool for Collapse Mechanism Analysis of Historic Masonry Structures, *International Journal of Architectural Heritage* (2018) 1–20doi:[10.1080/15583058.2018.1509155](https://doi.org/10.1080/15583058.2018.1509155).
- [8] T.-T. Bui, A. Limam, V. Sarhosis, Failure analysis of masonry wall panels subjected to in-plane and out-of-plane loading using the discrete element method, *European Journal of Environmental and Civil Engineering*doi:[10.1080/19648189.2018.1552897](https://doi.org/10.1080/19648189.2018.1552897).
- [9] J. Lemos, Discrete Element Modeling of the Seismic Behavior of Masonry Construction, *Buildings* 9 (43). doi:<https://doi.org/10.3390/buildings9020043>.
- [10] R. K. Varma, C. P. S. Tomar, S. Parkash, V. S. Sethi, Damage to brick masonry panel walls under high explosive detonations, *Pressure vessels and piping division. ASME* 351 (1997) 207 – 216.
- [11] B. Gabrielsen, C. Wilton, K. Kaplan, Response of arching walls and debris from interior walls caused by blast loading, Tech. rep., URS Reasearch Company, San Mateo. CA (1975).

- [12] S. T. Dennis, J. T. Baylot, S. C. Woodson, Response of 1/4-Scale Concrete Masonry Unit (CMU) Walls to Blast, *Journal of Engineering Mechanics* 128 (2) (2002) 134–142. doi:[10.1061/\(ASCE\)0733-9399\(2002\)128:2\(134\)](https://doi.org/10.1061/(ASCE)0733-9399(2002)128:2(134)).
- [13] B. M. Abou-Zeid, W. W. El-Dakhakhni, A. G. Razaqpur, S. Foo, Response of Arching Unreinforced Concrete Masonry Walls to Blast Loading, *Journal of Structural Engineering* 137 (10) (2011) 1205–1214. doi:[10.1061/\(ASCE\)ST.1943-541X.0000344](https://doi.org/10.1061/(ASCE)ST.1943-541X.0000344).
- [14] E. M. Gagnet, J. M. Hoemann, J. S. Davidson, Assessment of resistance definitions used for blast analysis of unreinforced masonry walls, *International Journal of Protective Structures* 8 (1) (2017) 125–151. doi:[10.1177/2041419617697518](https://doi.org/10.1177/2041419617697518).
- [15] R. A. Keys, S. K. Clubley, Experimental analysis of debris distribution of masonry panels subjected to long duration blast loading, *Engineering Structures* 130 (2017) 229 – 241. doi:<https://doi.org/10.1016/j.engstruct.2016.10.054>.
- [16] Z. Li, L. Chen, Q. Fang, H. Hao, Y. Zhang, H. Xiang, W. Chen, S. Yang, Q. Bao, Experimental and numerical study of unreinforced clay brick masonry walls subjected to vented gas explosions, *International Journal of Impact Engineering* 104 (2017) 107 – 126. doi:<https://doi.org/10.1016/j.ijimpeng.2017.02.002>.
- [17] G. Michaloudis, N. Gebbeken, Modeling masonry walls under far-field and contact detonations, *International Journal of Impact Engineering* 123 (2019) 84 – 97. doi:<https://doi.org/10.1016/j.ijimpeng.2018.09.019>.
- [18] P. Vannucci, I. Stefanou, F. Masi, *Cathédrales Durables*, Tech. rep., CNRS, Paris (2017).
- [19] P. Vannucci, F. Masi, I. Stefanou, A nonlinear approach to the wind strength of Gothic Cathedrals: The case of Notre Dame of Paris, *Engineering Structures* 183 (2019) 860 – 873. doi:<https://doi.org/10.1016/j.engstruct.2019.01.030>.
- [20] P. Vannucci, F. Masi, I. Stefanou, V. Maffi-Berthier, Structural integrity of Notre Dame Cathedral after the fire of April 15th, 2019, Submitted.
- [21] E. Whiting, H. Shin, R. Wang, J. Ochsendorf, F. Durand, Structural optimization of 3D masonry buildings, *ACM Transactions on Graphics (TOG)* 31 (6) (2012) 159.
- [22] C. Douthe, R. Mesnil, H. Orts, O. Baverel, Isoradial meshes: Covering elastic gridshells with planar facets, *Automation in Construction* 83 (2017) 222–236.
- [23] M. Wang, H. Hao, Y. Ding, Z.-X. Li, Prediction of fragment size and ejection distance of masonry wall under blast load using homogenized masonry material properties, *International Journal of Impact Engineering* 36 (6) (2009) 808 – 820. doi:<https://doi.org/10.1016/j.ijimpeng.2008.11.012>.
- [24] X. Wei, M. G. Stewart, Model validation and parametric study on the blast response of unreinforced brick masonry walls, *International Journal of Impact Engineering* 37 (11) (2010) 1150 – 1159. doi:<https://doi.org/10.1016/j.ijimpeng.2010.04.003>.
- [25] L. Macorini, B. A. Izzuddin, Nonlinear Analysis of Unreinforced Masonry Walls under Blast Loading Using Mesoscale Partitioned Modeling, *Journal of Structural Engineering* 140 (8) (2014) A4014002. doi:[10.1061/\(ASCE\)ST.1943-541X.0000931](https://doi.org/10.1061/(ASCE)ST.1943-541X.0000931).

- [26] S. H. Rafsanjani, P. Lourenço, N. Peixinho, Implementation and validation of a strain rate dependent anisotropic continuum model for masonry, *International Journal of Mechanical Sciences* 104 (2015) 24 – 43. doi:<https://doi.org/10.1016/j.ijmecsci.2015.10.001>.
- [27] F. Parisi, C. Balestrieri, D. Asprone, Blast resistance of tuff stone masonry walls, *Engineering Structures* 113 (2016) 233 – 244. doi:<https://doi.org/10.1016/j.engstruct.2016.01.056>.
- [28] Luís C. Silva and Paulo B. Lourenço and Gabriele Milani, Rigid block and spring homogenized model (HRBSM) for masonry subjected to impact and blast loading, *International Journal of Impact Engineering* 109 (2017) 14 – 28. doi:<https://doi.org/10.1016/j.ijimpeng.2017.05.012>.
- [29] I. Stefanou, K. Sab, J.-V. Heck, Three dimensional homogenization of masonry structures with building blocks of finite strength: A closed form strength domain, *International Journal of Solids and Structures* 54 (2015) 258 – 270. doi:<https://doi.org/10.1016/j.ijsolstr.2014.10.007>.
- [30] G. Andreotti, F. Graziotti, G. Magenes, Detailed micro-modelling of the direct shear tests of brick masonry specimens: The role of dilatancy, *Engineering Structures* 168 (2018) 929 – 949. doi:<https://doi.org/10.1016/j.engstruct.2018.05.019>.
- [31] E. G. Dimitrakopoulos, M. J. DeJong, Revisiting the rocking block: closed-form solutions and similarity laws, *Proceedings of the Royal Society of London A: Mathematical, Physical and Engineering Sciences* 468 (2144) (2012) 2294–2318. doi:[10.1098/rspa.2012.0026](https://doi.org/10.1098/rspa.2012.0026).
- [32] G. W. Housner, [The behavior of inverted pendulum structures during earthquakes](#), *Bulletin of the seismological society of America* 53 (2) (1963) 403–417.  
URL <http://resolver.caltech.edu/CaltechAUTHORS:20140801-112753969>
- [33] N. Makris, D. Konstantinidis, [The Rocking Spectrum and the Shortcomings of Design Guidelines](#), Tech. Rep. 2001/07, Pacific Earthquake Engineering Research Center, University of California, Berkeley, CA (2001).
- [34] F. Masi, I. Stefanou, P. Vannucci, V. Maffi-Berthier, Rocking response of inverted pendulum structures under blast loading, *International Journal of Mechanical Sciences* 157-158 (2019) 833 – 848. doi:<https://doi.org/10.1016/j.ijmecsci.2019.05.024>.
- [35] F. Masi, I. Stefanou, P. Vannucci, V. Maffi-Berthier, A discrete element method approach for the preservation of the architectural heritage against explosions, *Proceedings of the 12th International Congress on Mechanics Thessaloniki (HSTAM)*, Thessaloniki, Greece, 22-25 September.
- [36] Itasca Consulting Group, Inc., 3DEC 5.0 , Minneapolis, MN 55401 (2013).
- [37] P. B. Lourenço, L. F. Ramos, [Characterization of cyclic behavior of dry masonry joints](#), *Journal of Structural Engineering* 130 (5) (2004) 779–786.
- [38] L. F. R. Vélez, G. Magenes, M. C. Griffith, Dry stone masonry walls in bending—part i: Static tests, *International Journal of Architectural Heritage* 8 (1) (2014) 1–28. doi:[10.1080/15583058.2012.663059](https://doi.org/10.1080/15583058.2012.663059).

- [39] D. Malomo, M. J. DeJong, A. Penna, Distinct element modelling of the in-plane cyclic response of masonry walls subjected to shear-compression, *Earthquake Engineering & Structural Dynamics* doi:<https://doi.org/10.1002/eqe.3178>.
- [40] L. Freund, Crack propagation in an elastic solid subjected to general loading—i. constant rate of extension, *Journal of the Mechanics and Physics of Solids* 20 (3) (1972) 129 – 140. doi:[https://doi.org/10.1016/0022-5096\(72\)90006-3](https://doi.org/10.1016/0022-5096(72)90006-3).
- [41] L. Freund, Crack propagation in an elastic solid subjected to general loading—ii. non-uniform rate of extension, *Journal of the Mechanics and Physics of Solids* 20 (3) (1972) 141 – 152. doi:[https://doi.org/10.1016/0022-5096\(72\)90007-5](https://doi.org/10.1016/0022-5096(72)90007-5).
- [42] J. Weerheijm, Concrete under impact tensile loading and lateral compression, Ph.D. thesis, TU Delft, Delft University of Technology (1992).
- [43] C. A. Ross, J. W. Tedesco, S. T. Kuennen, Effects of strain rate on concrete strength, *Materials Journal* 92 (1) (1995) 37–47.
- [44] X. Chen, S. Wu, J. Zhou, Experimental Study on Dynamic Tensile Strength of Cement Mortar Using Split Hopkinson Pressure Bar Technique, *Journal of Materials in Civil Engineering* 26 (6) (2014) 04014005. doi:[10.1061/\(ASCE\)MT.1943-5533.0000926](https://doi.org/10.1061/(ASCE)MT.1943-5533.0000926).
- [45] A. M. Remennikov, A review of methods for predicting bomb blast effects on buildings, *Journal of Battlefield Technology* 6 (2003) 5–10.
- [46] M. Larcher, F. Casadei, Explosions in Complex Geometries — A Comparison of Several Approaches, *International Journal of Protective Structures* 1 (2) (2010) 169–195. doi:[10.1260/2041-4196.1.2.169](https://doi.org/10.1260/2041-4196.1.2.169).
- [47] D. Hyde, ConWep: Conventional weapons effects program, US Army Engineer Waterways Experiment Station, USA 2.
- [48] C. N. Kingery, G. Bulmash, Technical report ARBRL-TR-02555: Air blast parameters from TNT spherical air burst and hemispherical burst, Tech. rep., U.S. Army Ballistic Research Laboratory (1984).
- [49] P. Vannucci, F. Masi, I. Stefanou, [A study on the simulation of blast actions on a monumental structure](https://hal.archives-ouvertes.fr/hal-01447783v3/document). URL <https://hal.archives-ouvertes.fr/hal-01447783v3/document>
- [50] S. Wild, A. Gailius, H. Hansen, L. Pederson, J. Szwabowski, Pozzolanic properties of a variety of European clay bricks, *Building Research & Information* 25 (3) (1997) 170–175.
- [51] S. Petry, K. Beyer, Cyclic test data of six unreinforced masonry walls with different boundary conditions, *Earthquake Spectra* 31 (4) (2015) 2459–2484.
- [52] S. Petry, Force-displacement response of unreinforced masonry walls for seismic design, Tech. rep., École Polytechnique Fédérale de Lausanne, EPFL (2015).
- [53] S. Petry, K. Beyer, Scaling unreinforced masonry for reduced-scale seismic testing, *Bulletin of Earthquake Engineering* 12 (6) (2014) 2557–2581. doi:[10.1007/s10518-014-9605-1](https://doi.org/10.1007/s10518-014-9605-1).

- [54] T. Bui, A. Limam, Masonry walls under membrane or bending loading cases : experiments and Discrete Element analysis, Proceedings of the 11th International Conference on Computational Structures Technology, Dubrovnik, Croatia, 4–7 September.
- [55] E. Çaktı, Özden Saygılı, J. V. Lemos, C. S. Oliveira, [Discrete element modeling of a scaled masonry structure and its validation](#), Engineering Structures 126 (2016) 224 – 236. doi:<https://doi.org/10.1016/j.engstruct.2016.07.044>.  
URL <http://www.sciencedirect.com/science/article/pii/S0141029616303807>
- [56] T. Forgács, V. Sarhosis, K. Bagi, Minimum thickness of semi-circular skewed masonry arches, Engineering Structures 140 (2017) 317 – 336. doi:<https://doi.org/10.1016/j.engstruct.2017.02.036>.
- [57] J. Lemos, Numerical issues in the representation of masonry structural dynamics with Discrete Elements, Proceedings of the 1st ECCOMAS Thematic Conference on Computational Methods in Structural Dynamics and Earthquake Engineering (COMPDYN 2019), Papadrakakis, Fraiadakis (eds), Crete, Greece, 13–15 June (2007) 1126.
- [58] J. Lemos, Contact representation in rigid block models of masonry, International Journal of Masonry Research and Innovation 2 (2017) 321–334.